JOURNAL OF COMPUTATIONAL PHYSICS **145,** 316–331 (1998)
ARTICLE NO. CP986017

A New Parallel Solver for the Nonperiodic Incompressible Navier–Stokes Equations with a Fourier Method: Application to Frontal Polymerization[1]

M. Garbey and D. Tromeur-Dervout

Center for the Development of Parallel Scientific Computing CDCSP, University Lyon 1, Bât 101, 43 bd du 11 Novembre 1918, 69622 Villeurbanne, Lyon 69622, France
E-mail: mgarbey@cdcsp.univ-lyon1.fr and dtromeur@cdcsp.lyon1.fr

Received July 29, 1997; revised April 28, 1998

We present a specific use of domain decomposition and decomposition in function space combined with asymptotic analytical qualitative results to obtain, on parallel computers, efficient and accurate solvers [3] for rapidly varying quasi-planar unsteady combustion fronts in liquids. In particular, we give a *new parallel direct solver* of the unsteady incompressible Navier–Stokes equations in the stream function formulation. This solver is based on an embedding technique that allows us to generalize our previous results from the case with periodic boundary conditions [6, 7] to the *nonperiodic* case with wall boundary conditions in a direction perpendicular to front propagation. The solution is decomposed into a particular solution, suitable for a Fourier method, and the general homogeneous solution, calculated from an analytic solution with high precision, to satisfy the boundary conditions. The algorithm is implemented for parallel computers and results in a very effective code. Results on the effect of the convection onto the front propagation are provided.

Key Words: domain decomposition; Fourier expansions; Chebyshev polynomials; combustion; parallelism.

1. INTRODUCTION

Our applications to frontal polymerization (**FP**) are characterized by rapidly varying fronts and complex nonlinear dynamics. The multiple scale phenomena under consideration lead to very intense computations and can be analyzed formally by asymptotic methods [9, 8]. In this paper, we consider the propagation of reaction fronts in liquids that

[1] This work was backed by Région Rhône Alpes.

0021-9991/98 $25.00

models FP; FP is currently being investigated as a tool to design new materials that cannot be produced by classical processes [16]. The interaction between convective instabilities similar to Rayleigh Bénard's instability and thermal instabilities, well-known in solid phase combustion [15, 5] plays a key role in the modelization of FP [18, 17].

The aim of this paper is to give an algorithm that works for periodic, as well as for nonperiodic boundary conditions without changing the data structure, allowing us to extend our previous results [6] and maintaining the high accuracy required to produce reliable numerical simulations of FP. Instabilities in FP are very difficult computations to work out properly and extremely time consuming; we wholly use the very specific features of the solution that we are searching for and that corresponds to some experiments [16] to design our solver methodology. In addition, the basic idea of using local Fourier basis to go from periodic to nonperiodic boundary conditions with the same data structure and a good parallel efficiency might be of real interest for a more general situation [12–14, 4]. This paper gives a nontrivial example of the application of such methodology.

The outline of the present paper is as follows: First, we introduce the governing equations of our model of a 2D frontal polymerisation process in a liquid phase. Then in Section 2, we recall the special use of domain decomposition and decomposition in a function space, combined with asymptotic analytical qualitative results, to obtain, on parallel computers, efficient and accurate solvers [3] for rapidly varying quasi-planar unsteady combustion fronts in liquids with periodic boundary condition in the x direction. In Section 3 we give a *new parallel direct solver* of the unsteady incompressible Navier–Stokes, based on an embedding technique that allows us to generalize our previous results [6] from the periodic case to the *nonperiodic case*. The purpose of Section 4 is to provide an example of a numerical simulation made with our method and to illustrate the effectiveness of our approach. In this paper we have chosen to consider the effect of convection on the thermal instability of our combustion model. Conclusions are then given in Section 5.

1.1. *Governing Equations of a FP Process in a Liquid Phase*

The first step in modelization is to couple the reaction–diffusion system, well-known in solid combustion [15], with the Navier–Stokes equations written in the Boussinesq approximation. For the numerical simulation, we use the stream function–vorticity ($\Psi - \omega$) formulation of the N–S and we consider first-order one-step chemical reactions. C is the concentration of the reactant and T is the temperature. We look for special solutions of the dimensionless system (1)–(4)

$$\partial T/\partial t + (\partial\Psi/\partial z)(\partial T/\partial x) - (\partial\Psi/\partial x)(\partial T/\partial z) = \Delta T + W \tag{1}$$

$$\partial C/\partial t + (\partial\Psi/\partial z)(\partial C/\partial x) - (\partial\Psi/\partial x)(\partial C/\partial z) = \epsilon\Delta C - W \tag{2}$$

$$\partial\omega/\partial t + (\partial\Psi/\partial z)(\partial\omega/\partial x) - (\partial\Psi/\partial x)(\partial\omega/\partial z) = P\Delta\omega - RP\frac{\partial T}{\partial x} \tag{3}$$

$$\Delta\Psi = -\omega \tag{4}$$

that are traveling combustion fronts. W represents the source term given by the Arrhenius law,

$$W = ZC\exp\left(\frac{ZT}{1+\delta(1-T)}\right) \tag{5}$$

with $\delta = q/T_b$, ϵ a small parameter which is a scaled measure of the mass diffusion, P the Prandlt number, R the Rayleigh number, and $Z = qE/R_0 T_b^2$ the Zeldovich number, with R_0 the gas constant, E the activation energy, and q the adiabatic heat release, where $T_b = T_i + q$ is the adiabatic temperature and T_i is the temperature of the cold reactant.

The boundary conditions satisfied are

$$T \to 0, \quad C \to 1, \quad \omega \to 0, \quad \Psi \to 0, \quad \text{as } z \to -\infty, \tag{6}$$

$$T \to 1, \quad C \to 0, \quad \omega \to 0, \quad \Psi \to 0, \quad \text{as } z \to +\infty. \tag{7}$$

However, we solve (1)–(4) on the finite domain $\Omega = [-L, L] \times [0, 2\pi]$ with the boundary conditions

$$T(x, -L) = 0, \quad T(x, L) = 1 \qquad \text{for } x \in (0, 2\pi), \tag{8}$$

$$C(x, -L) = 1, \quad C(x, L) = 0 \qquad \text{for } x \in (0, 2\pi), \tag{9}$$

$$\omega(x, \mp L) = 0, \quad \Psi(x, \mp L) = 0 \quad \text{for } x \in (0, 2\pi), \tag{10}$$

and we take in the numerical simulation L large enough such that it has no influence on the dynamics of the combustion front.

Let us note that for this system (1)–(4) the derivation of the corresponding interface model [8] shows that in the limit of infinite activation energy the concentration exhibits a jump at the front, the temperature is continuous but it has a jump in its first-order derivative normal to the front, and the velocity is continuous, up to the third-order derivative normal to the front. Moreover, the viscosity of the N–S model is very low, so the stream function and consequently the vorticity do not show a TL near the front. Therefore the main difficulty in the computation is driven by the combustion process itself and not the computation of the flow.

The system (1)–(4) has one-dimensional traveling wave solutions that are stable or unstable, depending on the value of the bifurcation (and control) parameters Z, R, P, ϵ. We use these traveling wave solutions as initial conditions for the numerical simulation and introduce local perturbations to test their stability and/or to obtain new pattern formations of the solution. We maintain the time-dependent combustion front that propagates in the negative z direction during the numerical simulation roughly in the vicinity of the central line $x = 0$ by shifting in space the unknown functions. This shift is done by first computing the Chebyshev coefficients of the unknown functions, then shifting the computational grid in the z-direction: the unknown functions are interpolated at each point of the new computational grid, with spectral accuracy, except for new points of the physical domain which correspond to extrapolation. In addition, we satisfy (8)–(10) for all time. In the following paragraphs, we will consider two situations depending on the types of boundary conditions for the unknowns along the boundary $x = 0$ and $x = 2\pi$ of the domain. We recall that the solution exhibits multiple scale phenomena in space and in time: the combustion front is rapidly varying and the nonlinear source term W is close to a very sharp peak that drives the dynamic of the combustion reaction; the combustion front may pulse in time and its speed exhibits relaxation oscillations. The solution and its possible bifurcations are then intractable by low order schemes.

2. PERIODIC BOUNDARY CONDITIONS

Let us first briefly recall our methodology to solve the model problem [9, 8] with the periodic boundary conditions in the x variable. We use Chebyshev piecewise approximation

[10, 11] of the solution in the direction of propagation of the chemical wave (z variable) and Fourier expansion and/or high order finite differences in the periodic direction. Let us briefly describe the salient features of our method. A detailed description of the method can be found in [6].

We first consider the example of the scalar 1D equation:

$$\frac{\partial u}{\partial t} = \frac{\partial^2 u}{\partial z^2} + F_\epsilon(u), \quad u(-1) = 0,\ u(1) = 1, \tag{11}$$

with some appropriate initial condition. We suppose that u exhibits a *transition layer* (TL) of thickness ϵ located at $z = S(t) \in (-1, 1)$. It was shown in [1, 3, 10] that an efficient and accurate way to solve a TL is to use two subdomains with an interface located at the front and a mapping that concentrates the collocation points of the pseudo-spectral approximation at the end of the subdomains in the layer. The solution u of (11) restricted to one of these subdomains exhibits a boundary layer (BL) in the neighborhood of $S(t)$.

Let us consider that we have $nd = 2$ subdomains with N_z collocation points per subdomain and a semi-implicit Euler scheme for the integration in time:

$$\frac{u^{n+1} - u^n}{\Delta t} = D^2 u^{n+1} + F_\epsilon(u^n), \quad x \in \Omega_i,\ i = 1, 2, \tag{12}$$

where Δt is a constant time step, and D is the operator of differentiation. We take the second-order derivative term implicitly because it gives the main constraint on the time step. Since the nonlinear term is taken explicitly, u^{n+1} can be found as a solution to the linear system

$$\tilde{D} u^{n+1} = u^n + \Delta t F_\epsilon(u^n), \quad \text{with } \tilde{D} = \begin{pmatrix} A_1 & \hat{\beta} & \\ \tilde{\alpha}^t & \gamma & \tilde{\beta}^t \\ & \hat{\alpha} & A_2 \end{pmatrix}, \tag{13}$$

where γ is a real number, A_1 and A_2 are $(N_z - 1) \times (N_z - 1)$ matrices, $\hat{\alpha}, \hat{\beta}, \tilde{\alpha}^t, \tilde{\beta}^t$ are vectors with $(N_z - 1)$ components. The row $(\tilde{\alpha}^t, \gamma, \tilde{\beta}^t)$ appears from the condition of continuity of the first derivative at the interface. A_1 and A_2 correspond to the discrete operator $(I + \Delta t D^2)$ on each subdomain without the row acting on the interface points. The linear system (13) can eventually be solved with two parallel processes. The domain decomposition with two subdomains that we have presented here can be generalized to an arbitrary number of subdomains to solve multiple front structures [3, 1]. This domain decomposition is a **first level of decomposition** that is, a priori, a nonscalable parallelism because of its dependence on the numbers of the layers. As the front moves we adapt the grid in the z-direction in order to put the interface of the two subdomains at the sharp position of the front. The location of the front is derived from asymptotic criteria and/or an a priori estimate.

To move toward a **second level of decomposition** that uses a fine grid level of parallelism, we shall now consider a two-dimensional case with some appropriate initial conditions, thus generalizing our previous example (11):

$$\begin{gathered} \partial u/\partial t = \partial^2 u/\partial x^2 + \partial^2 u/\partial z^2 - F_\epsilon(u), \quad z \in (-1, 1),\ x \in (0, 2\pi), \\ u(x, -1) = 0, \quad u(x, 1) = 1, \quad x \in (0, 2\pi). \end{gathered} \tag{14}$$

We look for a periodic solution $u(z, x)$ in the x variable. We now assume that the TL of the problem (14) depends *weakly* on x. This hypothesis significantly simplifies the technique of the domain decomposition method as we will see in the following. As the solution u is not rapidly varying in the x direction, we can use a regular mesh in the x-direction. Our first choice is to use a central finite-difference scheme of order 6 for D_x^2, the approximation of $\partial^2/\partial x^2$, on a regular grid of N_x points with a step $h = 2\pi/(N_x - 1)$. The finite difference approximation of order 6 of the term $\partial^2 u/\partial x^2$ is treated *explicitly*. The cost of the algorithm is very low because the complexity of the computation is linear with respect to N_x. In addition, the time step constraint due to the explicit treatment of the second order derivative is, in practice, of the same order as the time step restriction due to the explicit treatment of the nonlinear source terms. The numerical algorithm can exploit the fine grid decomposition due to the explicit dependence on x because the computation of $D_x^2 u^n$ is used with an explicit formula which only includes local values of the function u^n.

Let us now consider the steady state equation analogous to (14), i.e.,

$$\frac{\partial^2 u}{\partial x^2} + \frac{\partial^2 u}{\partial z^2} = F_\epsilon(x, z), \quad u(x, -1) = 0, \quad u(x, 1) = 1, \quad z \in (-1, 1),\ x \in (0, 2\pi). \quad (15)$$

We now need to use an implicit approach, with respect to *both* space variables. We look for the x-periodic function $u(z, x)$ as a discrete Fourier expansion:

$$u(x, z) = \Sigma_{k=-N_x/2, N_x/2-1}\, \hat{u}_k(z)\, e^{ikx}. \quad (16)$$

We compute the Fourier modes $\hat{F}_k(z)$ of the $F_\epsilon(z, x)$ function. Then the functions $\hat{u}_k(z)$ can be found from the system of N_x *independent* ordinary differential equations:

$$\frac{\partial^2}{\partial z^2}\hat{u}_k(z) - k^2 \hat{u}_k(z) = \hat{F}_k(z), \quad k = \frac{-N_x}{2}, \frac{N_x}{2} - 1. \quad (17)$$

These equations are solved with the same one-dimensional domain decomposition method in z-direction as described above (Eq. (13) with $\tilde{D} = -k^2 I + D^2$). We then have a fine grid level of parallelism with respect to the wave number k. We have implemented these techniques to solve the problem (1)–(4) with periodic boundary conditions. Using nonblocking communications we obtained an efficiency of about 90% with $nd = 2$, $N_x = 128$, $N_z = 59$ on the paragon with 32 nodes. We refer to [6] for a detailed description of the results. Our second choice is to use a similar parallel scheme to compute the time dependent problem (14) as well; but we observe that the complexity of the algorithm with respect to N_x becomes quadratic when using a matrix product approach. In addition the algorithm requires a global transposition of the data that might affect the efficiency of the parallel algorithm.

3. DECOMPOSITION IN FUNCTION SPACE FOR THE NONPERIODIC BOUNDARY CONDITIONS

The next step to obtain a more realistic model, is to include the nonperiodic boundary conditions (BC), because the walls of the test tubes may significantly influence the dynamics of the combustion front [16]. We consider homogeneous Neuman boundary conditions for the concentration and possible heat transfer for the temperature at the walls. Eqs. (1) to (2) can be solved with the same method as above, except that the finite differences with

respect to x must be modified to implement the new boundary conditions. However, our solution of the stream function equation uses the Fourier expansion in the x-direction and this cannot be applied to the case of the nonperiodic boundary conditions. It is quite possible to substitute into the Fourier approximation a Chebyshev approximation of Ψ and ω in the x-direction as well, but this will result in a large change of the data structure of the code and will give rise to difficulties in terms of parallelism efficiency. Our objective is to build an efficient parallel numerical scheme that works with periodic, as well as nonperiodic (BC) problems **with the same data structure**. To achieve this goal we develop a technique, that is an extension of the work of Israeli *et al.* [13]. Let us consider the unsteady incompressible Navier–Stokes equation, on the domain $\Omega =]0, 2\pi[\times]-L, +L[$, written in stream function formulation with a no-slip boundary condition along the vertical walls $x = 0, z \in (-L, L)$, and $x = 2\pi, z \in (-L, L)$:

$$\begin{aligned} \partial\Delta\Psi/\partial t &= (\partial\Psi/\partial x)(\partial\Delta\Psi/\partial z) - (\partial\Psi/\partial z)(\partial\Delta\Psi/\partial x) \\ &\quad + \Delta\Delta\Psi - f(x, z, t), \quad (x, z) \in \Omega, \\ \Psi(0, z) &= 0, \quad (\partial\Psi/\partial x)(0, z) = 0, \qquad z \in (-L, L), \\ \Psi(2\pi, z) &= 0, \quad (\partial\Psi/\partial x)(2\pi, z) = 0, \quad z \in (-L, L). \end{aligned} \tag{18}$$

We are going to use a special feature of our model problem (1)–(4) on the infinite strip $(0, 2\pi) \times (-\infty, \infty)$; the gradient of the temperature vanishes exponentially far from the combustion front for large z. Therefore $f(x, z, t) = RP(\partial T/\partial x)$ is vanishing exponentially and consequently Ψ and its derivatives are vanishing exponentially for large z, too. We can look at Ψ as a smooth periodic function in the z-direction of period $2L$. Therefore, a Fourier expansion of Ψ in the z-direction does not exhibit a Gibbs phenomena. We will in practice take L large enough in our numerical simulation such that it has no influence on the computed combustion front.

Let us consider the following semi-implicit Euler scheme for iterating in time:

$$\begin{aligned} \Delta\Psi^{n+1} - dt\Delta\Delta\Psi^{n+1} &= dt((\partial\Psi^n/\partial x)(\partial\Delta\Psi^n/\partial z) - (\partial\Psi^n/\partial z)(\partial\Delta\Psi^n/\partial x) \\ &\quad + \Delta\Psi^n - dt\, f(x, z, t_n), \quad (x, z) \in \Omega, \\ \Psi^{n+1}(0, z) &= 0, \quad (\partial\Psi^{n+1}/\partial x)(0, z) = 0, \qquad z \in (-L, L), \\ \Psi^{n+1}(2\pi, z) &= 0, \quad (\partial\Psi^{n+1}/\partial x)(2\pi, z) = 0, \quad z \in (-L, L). \end{aligned} \tag{19}$$

We use a spectral method in Fourier space in the z-direction; f and Ψ at time t_n are approximated by the following discrete Fourier expansion:

$$f(x, z, t_n) = \Sigma_{k=-N_x/2, N_x/2-1} \hat{f}_k^n(x)\, e^{iky}, \tag{20}$$

$$\Psi^n(x, z, t_n) = \Sigma_{k=-N_x/2, N_x/2-1} \hat{\Psi}_k^n(x)\, e^{iky}, \tag{21}$$

$$y = \frac{(z + L)\pi}{L}. \tag{22}$$

Let us denote by $F^n(x, z)$ the right-hand side of Eq. (19). From the approximation

$$\begin{aligned} &(\partial\Psi^n/\partial x)(\partial\Delta\Psi^n/\partial y) - (\partial\Psi^n/\partial y)(\partial\Delta\Psi^n\partial x) \\ &\quad \approx i\,\Sigma_{k=-N_x/2, N_x/2-1}\big[e^{iky}\,\Sigma_{k_1+k_2=k}\big(\hat{\Psi}_{k_1}^{n'} k_2\big(\hat{\Psi}_{k_2}^{n''} - k_2^2\hat{\Psi}_{k_2}^n\big) - \hat{\Psi}_{k_1}^n k_1\big(\hat{\Psi}_{k_2}^{n'''} - k_2^2\hat{\Psi}_{k_2}^{n'}\big)\big)\big], \end{aligned} \tag{23}$$

we obtain the discrete Fourier expansion of F^n. We have then to solve at each time step the uncoupled fourth-order N_x ODE's:

- for $k = 0$:

$$\left(\hat{\Psi}_0^{n+1}\right)'' - dt\left(\hat{\Psi}_0^{n+1}\right)'''' = \hat{F}_0^n, \quad x \in (0, 2\pi), \tag{24}$$

$$\hat{\Psi}_0^{n+1}(0) = \left(\hat{\Psi}_0^{n+1}\right)'(0) = \hat{\Psi}_0^{n+1}(2\pi) = \left(\hat{\Psi}_0^{n+1}\right)'(2\pi) = 0. \tag{25}$$

- for $k \neq 0$:

$$\left(\hat{\Psi}_k^{n+1}\right)'' - k^2\hat{\Psi}_k^{n+1} - dt\left(\left(\hat{\Psi}_k^{n+1}\right)'''' - 2k^2\left(\hat{\Psi}_k^{n+1}\right)'' + k^4\hat{\Psi}_k^{n+1}\right) = \hat{F}_k^n, \quad x \in (0, 2\pi), \tag{26}$$

$$\hat{\Psi}_k^{n+1}(0) = \left(\hat{\Psi}_k^{n+1}\right)'(0) = \hat{\Psi}_k^{n+1}(2\pi) = \left(\hat{\Psi}_k^{n+1}\right)'(2\pi) = 0. \tag{27}$$

Let us formally denote these fourth-order *linear* ODE equations

$$L_k\left[\hat{\Psi}_k^{n+1}\right] = \hat{F}_k^n, \quad x \in (0, 2\pi). \tag{28}$$

The main idea is to *also* compute $\hat{\Psi}_k^{n+1}$ with Fourier expansion. We will omit the subscript k and $n+1$ to simplify the notations in what follows. Using the superposition principle, the solution $\hat{\Psi}$ is written

$$\hat{\Psi} = \hat{\Psi}_F + \hat{\Psi}_C, \tag{29}$$

where $\hat{\Psi}_F$ and $\hat{\Psi}_C$ are defined in the next sections.

3.1. *The Particular Solution $\hat{\Psi}_F$ with Fourier*

Let $d > 0$, $d \in \mathbf{R}$, and let $[0, 2\pi + d]$ be an extension of the domain $(0, 2\pi)$. Then if $\hat{F}$ is in $C^n(0, 2\pi)$ there exists $\bar{F}$ in $C^n(0, 2\pi + d)$ that is an x-periodic extension of $\hat{F}$. We construct $\bar{F}$ as follows. We consider the exact or computed values of the derivatives of $\hat{F}$ until order nth at $x = 0$ and $x = 2\pi$. The classical Hermite interpolation allows us to define a polynomial function $P_{\hat{F}}$ on $[2\pi, 2\pi + d]$ of degree $2n + 1$ that interpolates the function $\hat{F}$ with the conditions:

$$\begin{aligned} &P_{\hat{F}}^{(0)}(2\pi) = \hat{F}^{(0)}(2\pi), \quad P_{\hat{F}}^{(1)}(2\pi) = \hat{F}^{(1)}(2\pi), \ldots, \quad P_{\hat{F}}^{(n)}(2\pi) = \hat{F}^{(n)}(2\pi), \\ &P_{\hat{F}}^{(0)}(2\pi + d) = \hat{F}^{(0)}(0), \quad P_{\hat{F}}^{(1)}(2\pi + d) = \hat{F}^{(1)}(0), \ldots, \quad P_{\hat{F}}^{(n)}(2\pi + d) = \hat{F}^{(n)}(0). \end{aligned} \tag{30}$$

Then the x-periodic function $\bar{F}$ of period $2\pi + d$ is given as

$$\bar{F}(x) = \begin{cases} \hat{F}(x) & \forall x \in [0, 2\pi], \\ P_{\hat{F}}(x) & \forall x \in [2\pi, 2\pi + d]. \end{cases} \tag{31}$$

We then define Ψ_F as the solution of the problem:

$$\begin{gathered} L_k[\hat{\Psi}_F] = \bar{F}, \quad x \in (0, 2\pi + d), \\ \hat{\Psi}_F \; 2\pi + d \text{ periodic} \\ \hat{\Psi}_F \in C^{n+4}(\mathbf{R}). \end{gathered} \tag{32}$$

3.2. *Corrector Term:* $\hat{\Psi}_C$

We observe that (28) is a singular perturbation problems with $dt = O(1)$ as a singular perturbation parameter, and $\hat{\Psi}_F$ is a regular expansion of the solution [2]. The next step consists in searching for a corrector $\hat{\Psi}_C$ so that $\hat{\Psi}$ may satisfy Eq. (28) on the domain Ω with the correct boundary conditions, i.e.,

$$\begin{aligned} L_k[\hat{\Psi}_C] &= 0, \quad x \in (0, 2\pi), \\ \hat{\Psi}_C(0) &= -\hat{\Psi}_F(0), \qquad (\hat{\Psi}_C)'(0) = -(\hat{\Psi}_F)'(0) \\ \hat{\Psi}_C(2\pi) &= -\hat{\Psi}_F(2\pi), \quad (\hat{\Psi}_C)'(2\pi) = -(\hat{\Psi}_F)'(2\pi). \end{aligned} \tag{33}$$

Since the operators, L_k are fourth-order linear operators with constant coefficients, one can once and for all compute the basis for the fourth-dimensional vector space of the solutions; so we have

- for $k = 0$:

$$\hat{\Psi}_C^0 = \alpha_0\, e^{-(x/\sqrt{dt})} + \beta_0\, e^{-((2\pi - x)/\sqrt{dt})} + \gamma_0 x + \delta_0(2\pi - x); \tag{34}$$

- for $k \neq 0$:

$$\hat{\Psi}_C^k = \alpha_k\, e^{-|k|x} + \beta_k\, e^{-|k|\,(2\pi - x)} + \gamma_k\, e^{-(\sqrt{k^2 + (1/dt)}x)} + \delta_k\, e^{-(\sqrt{k^2 + (1/dt)}(2\pi - x))}. \tag{35}$$

The derivatives of $\hat{\Psi}_C^k$ can be computed readily from the previous formulae. The derivatives of $\hat{\Psi}_F^k$ can be computed from its discrete Fourier expansion. We assemble the right-hand side of Eq. (19) at each time step using the splitting (29) on the derivatives as well.

3.3. *Results and Algorithm*

Our technique differs essentially from the work of Israeli *et al*. [13], by the way we extend the right-hand side (RHS) of our ODEs problems; they use a so-called bell function that cuts off the RHS into zero outside $(0, 2\pi)$. We find improved accuracy using Hermite interpolation even if the derivatives of $\hat{F}$ are computed numerically via decentered finite differences. In practice, we use Hermite interpolation up to second-order derivatives. In addition the work of Israeli *et al*. is focused on the Helmholtz problem, but there are several new difficulties to properly implement the method when a nonlinear time-dependent problem is solved. We refer to [4] for a detailed study of this method applied to a large set of classical problems.

We have tested the stability and accuracy of our numerical scheme to solve the biharmonic problem on $\Omega =]0, L_x[\times]-L, +L[$ as the steady limit of the problem:

$$\begin{aligned} \partial \Delta \Psi / \partial t &= \Delta \Delta \Psi - f(x, z, t), \qquad (x, z) \in \Omega, \\ \Psi(0, z) &= 0, \quad (\partial \Psi / \partial x)(0, z) = 0, \qquad z \in (-L, L), \\ \Psi(L_x, z) &= 0, \quad (\partial \Psi / \partial x)(L_x, z) = 0, \quad z \in (-L, L). \end{aligned} \tag{36}$$

We have determined the source term f in order to have an exact solution that satisfies the equation, as well as the boundary conditions. The dimension of the domain is $L_x = \pi$ in the x-direction and $2L = 2\pi$ in the z-direction. The number $N_x/2$ denotes the number of modes in x-direction used on the extended domain. We have imposed C^2 continuity conditions to build the Hermite interpolation polynomial (i.e., $n = 2$ in (30)). The numerical values

TABLE I

Error in Maximum Norm between the Exact Solution $\pi^{-5}(x-\pi)^2x^3$ and the Computed Solution with Respect to the Number of Modes $N_x/2$ and the Ratio between the Extended Domain and the Original Domain

	Solution: $\pi^{-5}(x-\pi)^2x^3$		
$\frac{N_x}{2}$	$\frac{L_x+d}{L_x}=2$	$\frac{L_x+d}{L_x}=1.1429$	$\frac{L_x+d}{L_x}=1.0667$
8	0.205213E−02	0.950714E−02	0.721939E+01
16	0.817644E−04	0.984945E−04	0.142515E−02
32	0.188141E−05	0.255054E−05	0.158448E−04
64	0.344994E−07	0.932849E−07	0.233131E−06
128	0.421207E−09	0.198517E−08	0.829286E−08

of the derivatives involved in the Hermite conditions (30) are computed with one-sided second-order finite differences, based on grid points inside the physical domain. It is not wise to use central finite differences because the Gibbs phenomenon might be amplified by the interpolation process after each time step.

Tables I and II give the maximum norm of the error between the computed solution and the exact solution with respect to the number of modes $N_x/2$ for two test cases. In addition, we test the influence of the ratio $(L_x+d)/L_x$ between the size L_x+d of the extended domain and the size L_x of the physical domain on the accuracy.

The exact solutions, defined on $[0, L_x]\times[-\pi,\pi]$, are not periodic in the x-direction and are chosen such that their maximum value is equal to 1. Table I corresponds to a gradually varying polynomial test function, but in Table II we consider a more rapidly varying test function. The time step is a matter of choice since we only test the steady limit, but it has obviously some influence on the stability and accuracy of the scheme. This is discussed below, and Tables I and II have been obtained with $\Delta t = 10^{-2}$.

We note that the speed of convergence of the method is at least of order 4 for Table II results and of order 5 for Table I results. In fact when one considers only the results for

TABLE II

Error in Maximum Norm between the Exact Solution $\pi^{-5}(x-\pi)^2x^3e^{8(\sin(z)-1)}$ and the Computed Solution with Respect to the Number of Modes $N_x/2$ and the Ratio between the Extended Domain and the Original Domain

	Solution: $\pi^{-5}(x-\pi)^2x^3e^{8(\sin(z)-1)}$		
$\frac{N_x}{2}$	$\frac{L_x+d}{L_x}=2$	$\frac{L_x+d}{L_x}=1.1429$	$\frac{L_x+d}{L_x}=1.0667$
8	0.112976E−01	0.868233E+00	0.123936E+01
16	0.672073E−03	0.210331E−01	0.804409E+00
32	0.326011E−04	0.757420E−03	0.566257E−02
64	0.168978E−05	0.437461E−04	0.176142E−04
128	0.947167E−07	0.229509E−05	0.632574E−06

the larger values of N_x in Tables I and II the results seem to get closer to order 6. This felicitous convergence is in agreement with the fact that for each mode k the right-hand side of the fourth-order equation satisfied by Ψ_F^k is extended as a $C^2(0, 2\pi + d)$ function: Ψ_F^k is, therefore, in $C^6(0, 2\pi + d)$. However, since the extension of the right-hand side is built numerically, it is not obvious at all. In addition, we observe that the size of the extended domain has less and less influence on the accuracy of the solution when the number of Fourier modes is large enough. This observation is in agreement with the 1D theory of the method [4].

We must emphasize that the discrete Fourier expansion of the corrector

$$\Psi_C^n(x, z) = \Sigma_{k=-N_x/2, N_x/2-1} \hat{\Psi}_{C,k}^n(x)\, e^{iky}, \quad y = \frac{(z + L)\pi}{L}$$

exhibits at leading order, more precisely for $k \in (-1/\sqrt{dt}, 1/\sqrt{dt})$, a boundary layer of $O(\sqrt{dt})$ thickness. We have observed some spurious oscillations related to the Gibbs phenomenon, when the time step is so small that the physical space step does not allow a good representation of the layer. For the gradually varying test function of Table I, for example, $\Delta t = 5 \times 10^{-4}$ seems to be the smallest time step that allows numerical convergence with 32 Fourier modes. A smaller time step leads to blowup. The obvious thing to do to overcome this difficulty should be to use optimal filters, but this was not required for our numerical simulation in the combustion described below.

The parallel implementation of our new solver consists in distributing the mode equations between the processors. So each processor has to solve a set of equations for several modes and then gathers the modes to build that part of the solution belonging to its computational domain. The algorithm corresponding to our new parallel solver for the Navier–Stokes equations can be summarized for each time step as follows:

- Step 1. Compute $\hat{F}_k^n$.
- Step 2. Extend $\hat{F}_k^n$.
- Step 3. Compute the explicit formula for α_k, β_k, γ_k, δ_k.
- Step 4. Compute $\hat{\Psi}_{F,k}$ via a matrix product approach.
- Step 5. Add the corrector $\hat{\Psi}_{C,k}$ to the periodic solution where it is not negligible.

We observe that the efficiency of the parallel implementation depends crucially on the first step because of the coupling of the different modes. Since Step 1 is a piece of the computation of Eqs. (1), (2), and (18), independent of C, communications can be conveniently overlapped by computation. On the contrary, Steps 2 to 5 of the algorithm are fully parallel.

We have been able to obtain good efficiency (90%) from this method on a four-processor alpha server, just by unrolling the loop on the modes. Experiments with MPI and larger numbers of processors are currently in progress. However, it is not critical for our applications because a Dec alpha server with four 400-Mhz processors is at least 50% as fast as a 32-node paragon [7].

We note that in order to calculate the right-hand side $f(x, z, t)$ of Eq. (19) on the grid (x-uniform, z-Chebyshev), the term $\partial T/\partial x$ must be interpolated in the z-direction from the (x-uniform, z-Chebyshev) grid to the (x-uniform, z-uniform) grid. The computed Ψ solution must be interpolated back. Each of these distributed interpolations are performed with collocating the unknown function on the spectral grid points and evaluating its polynomial representation on the other grid points. The time spent in each of these two interpolations

is respectively 3% and 3.6% of the total time per iteration on four processors for the frontal polymerisation problem described below.

Remark. The matrix multiply approach for the number of Fourier modes that we consider is very effective on our Dec alpha computer; however, one should consider parallel FFT solvers for larger problems.

4. A RESULT ON FRONTAL POLYMERISATION

A systematic investigation of the nonperiodic boundary condition effects on convective and thermal instabilities of the combustion model under consideration is beyond the scope of this paper, so we have selected here a numerical simulation that illustrates the numerical effectiveness of our method.

Specifically, we show the effect of convection on the thermal instability that can also exist without convection, that is when $R = 0$. This computation was done in the following way:

We start with the values of parameters, where the thermal instability occurs, Zeldovich number $Z = 7.8$ and a domain of a width 4π. The time-periodic pattern of the combustion front can be described briefly as follows: the solution stays symmetrical in space around the medium line $x = 2\pi$ at all time; a hot spot attached to the front and located on the axis of symmetry of the solution, successively splits into two hot spots that propagate rapidly against the walls and then form again when the two hot spots come back simultaneously from the walls and merge. This type of instability is well known in solid combustion; it was observed in SHS experiments and analyzed with asymptotic methods [21, 20, 19].

Starting from this initial solution, we introduce the effect of convection in this numerical simulation by gradually increasing the Rayleigh number from $R = 0$; positive Rayleigh numbers correspond to ascending fronts. The exothermic reaction front heats the fresh reactant from below and we can expect the appearance of convection rolls. For this computation, we use $nd = 2$ subdomains with 59 Chebyshev collocation points in the z-direction, 80 modes in the x-direction, an extension domain ratio of 1.2850 for the stream-function solution and 128 finite differences points in x-direction for the other unknowns.

Figure 1 represents the x-location of the hot spot with respect to time for the FP with and without hydrodynamics (respectively $R = 5$ and $R = 0$). Because the solution is symmetric with respect to $x = \pi$, we can omit the representation of the solution for $R = 0$ (respectively $R = 5$) in the lower half (respectively the upper half) of the domain of computation.

The period in time of the FP process with $R = 5$ (resp. $R = 0$) is measured to be 3.99 (resp. 3.66) time units; the maximum value for all times of the hot spot is 1.285 (resp. 1.1635). The convective effects have slowed down the FP process.

The mechanism of propagation of the hot spot deals with the interaction of reaction and diffusion processes. When the hot spot on the central line decreases and the two hot spots along the wall increase there is a specific time when the location of the maximum value of the temperature jumps from the central line to the location near the walls; it corresponds to a vertical line in Fig. 1.

In order to measure the different phases in the FP process and analyze the effect of convection we can define the following events:

- A: the hot spot leaves the center of the domain
- B: the hot spot reaches the walls

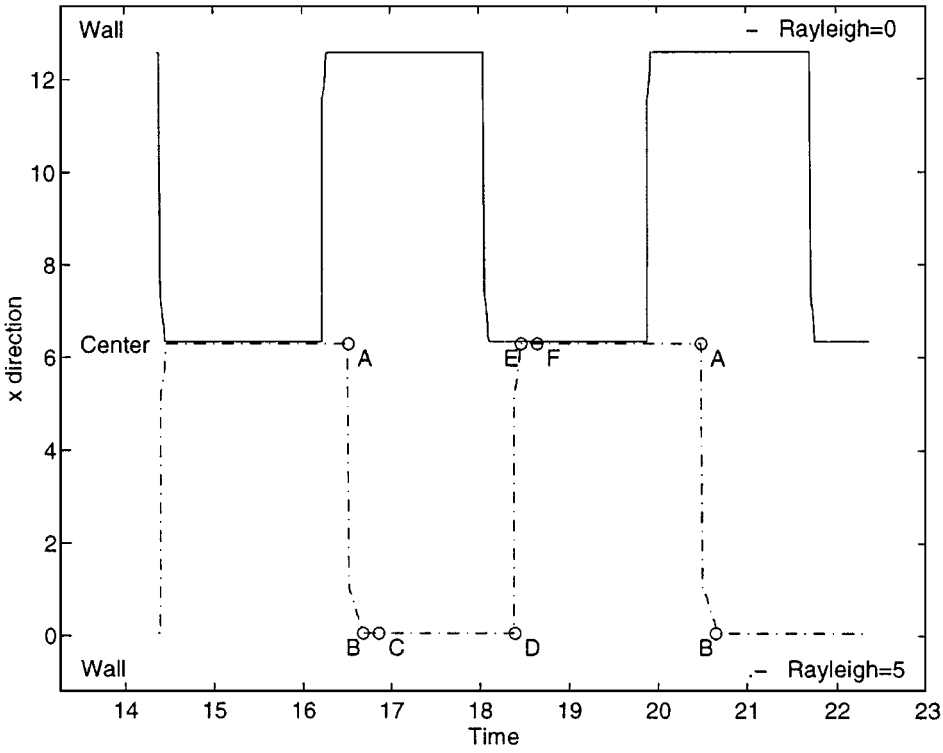

FIG. 1. Comparison of the motion of the hot spot along the x-direction in time with hydrodynamics ("-.-," $R = 5$, lower half part of the domain) and without hydrodynamics ("-," $R = 0$, upper half part of the domain).

- C: the hot spot reaches its maximum value in time during the time period when it stays close to the wall
- D: the hot spot leaves the walls
- E: the hot spot reaches the center of the domain
- F: the hot spot reaches its maximum value in time for all time.

It clearly appears that the convection:

1. slows down the FP propagation
2. breaks the symmetry of the time period since the hot spot stays longer along the central line than along the wall. This is not the case when $R = 0$.
3. increases the maximum value of the hot spot.
4. slows down the diffusion of the hot spot strongly in the direction from the center to the wall and weakly in the direction from the wall to the center.
5. speeds up the motion of the two hot spots in the direction from the wall to the center and from the center to the wall.

This can be understood somehow by looking at the interaction between the spatial structure of the temperature field and the corresponding hydrodynamic structures when $R = 5$ —see Figs. 2 and 3. The dashed lines represent the stream-function isovalues, while the solid lines represent the temperature isovalues. We superpose the two fields on the same

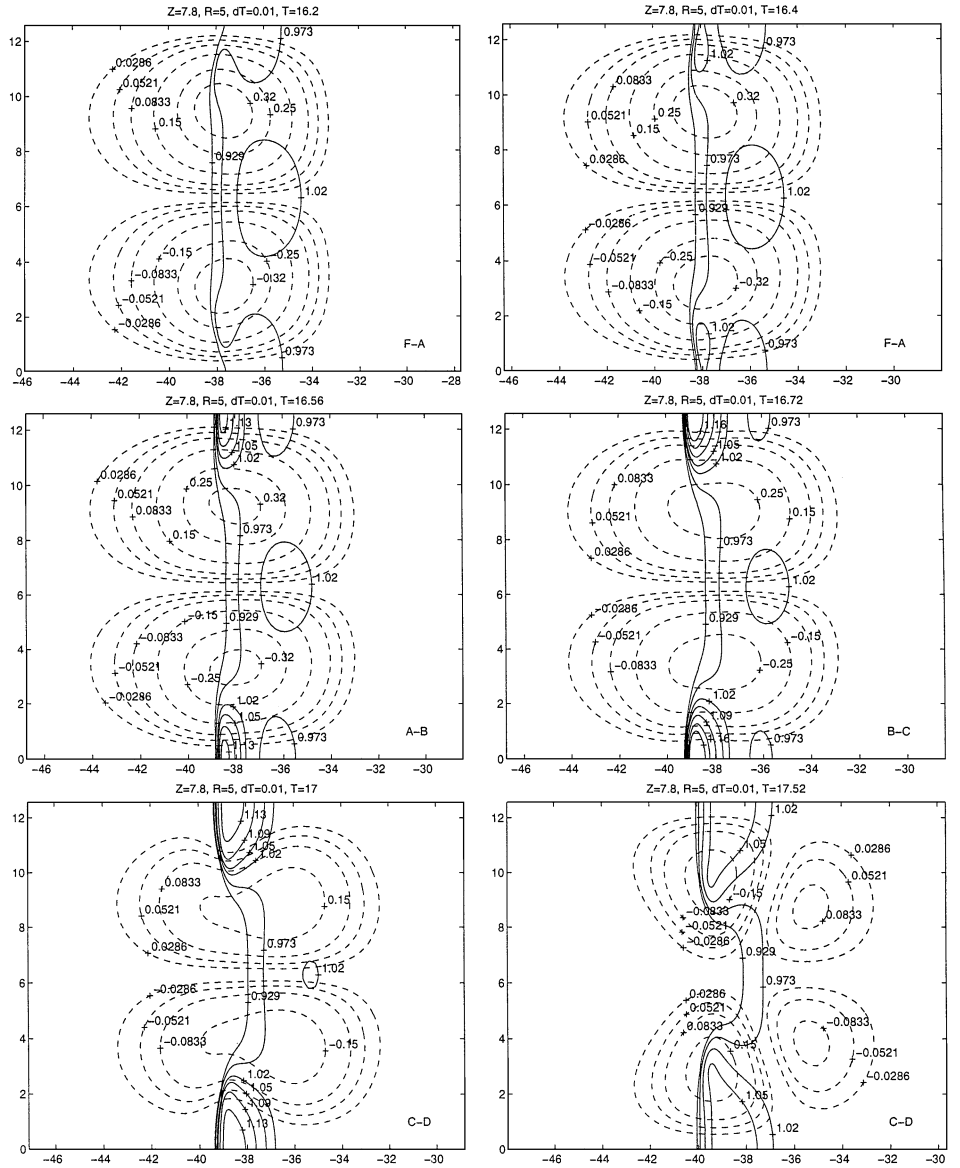

FIG. 2. Evolution with time of the isovalues of the temperature (solid line) and the isolvalues of the stream function (dash line). Reference to the time event of Fig. 1 is given in the bottom right hand corner.

pictures in order to better show the coupling between the convection and gradient of temperatures (Boussinesq approximation (3)). The symmetry of the stream function is satisfied to the fourth digit.

During the phase E–F, the flow structure, generated by the hot spot, transports some heat to the fresh reactant. This preheat increases the combustion process, leading to a rise in the value of the hot spot at the center of the combustion front ($T = 18.36$, 18.44, and 18.56). When this hot spot ($T = 18.56$) reaches the maximum value (1.285), it diffuses in the x-direction ($T = 19.0$, 19.6, and 16.2, phase F–A) and creates new flow structures with an opposite spin as the previous ones. Then the two oldest flow structures die, due to the

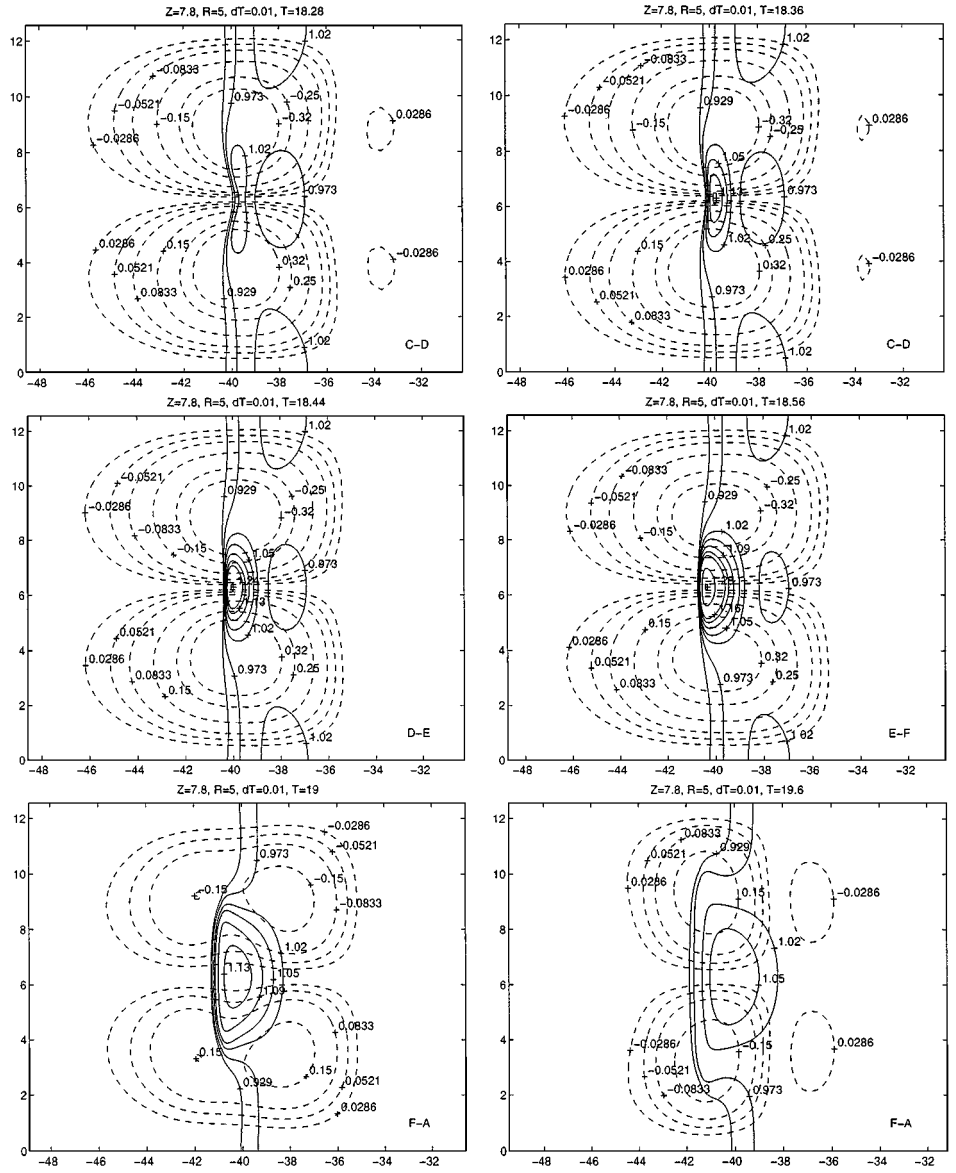

FIG. 3. Evolution (continued) with time of the isovalues of the temperature (solid line) and the isolvalues of the stream function (dash line). Reference to the time event of Fig. 1 is given in the bottom right hand corner.

opposite spin of the vortices attached to the hot spots. In the sequel, the hot spot splits into two hot spots which join the walls ($T = 16.4$ and $T = 16.56$, phases A–B).

A new flow structure is then established ($T = 16.56$ and $T = 16.72$, phase B–C). The fluid motion transports some heat to the fresh reactant located at the center of the domain that contributes to increase the hot spot values. The hot spots attached to the front propagate along the wall. When the hot spots reach a maximum value of 1.21 ($T \simeq 16.72$, phase C–D), they diffuse toward the center of the front ($T = 17.0, 17.52, 18.28$, phase D–E) and merge ($T = 18.36$), creating two new vortices with an opposite spin to the previously established flow structure of phase B–C.

TABLE III
Elapsed Time between the Events A and B, B and C, etc. of the FP with and without Hydrodynamics

Time	A-B	B-C	C-D	D-E	E-F	F-A	Period
R = 0	0.04	0.34	1.45	0.04	0.34	1.45	3.66
R = 5	0.16	0.18	1.54	0.08	0.18	1.85	3.99

Note. Rayleigh number R = 5 and R = 0, respectively.

5. CONCLUSION

We have presented a new algorithm that allows us to generalize our previous results in the modelization of frontal polymerization with the classical simplification of periodicity to nonperiodic boundary conditions.

Our technique relies on combining complementary levels of decomposition according to the asymptotic properties of the combustion model and the specific structure of the traveling waves under consideration. These techniques are developed to make an efficient use of MIMD architecture using among other concepts, a parallelism based on the Fourier modes decomposition.

We have numerically shown for some test functions that this technique can be of order 4 at least and that the length of the domain extension has little influence on the solution accuracy for large numbers of modes.

We have given a nontrivial illustration of this method with a numerical simulation that couples convection motion of the fluid and the well-known thermal instability of a combustion front.

We are currently investigating the possibilities of generalizing of this embedding technique to solve free boundary problems that occur in liquid–solid frontal polymerisation [9].

ACKNOWLEDGMENT

The authors thank D. Gottlieb, J. Pojman, and V. Volpert for many interesting discussions on the present work. We also thank one of the reviewers for many constructive comments.

REFERENCES

1. A. Bayliss, M. Garbey, and B. Matkowsky, Adaptive pseudo-spectral domain decomposition method and the approximation of multiple layers, *J. Comput. Phys*. **119**, 132 (1995).
2. W. Eckhaus, *Asymptotic Analysis of Singular Perturbations* (North-Holland, Amsterdam, 1979).
3. M. Garbey, Domain decomposition to solve transition layers and asymptotic, *SIAM J. Sci. Comput*. **15**(4), 866 (1994).
4. M. Garbey, On some applications of the superposition principle with (local) fourier basis, Preprint CDCSP-97-02, submitted.
5. M. Garbey, H. Kaper, G. Leaf, and B. Matkowsky, Using maple for the analysis of bifurcation phenomema in condensed phase surface combustion, *J. Sci. Comput.* **12**, 89 (1991).
6. M. Garbey and D. Tromeur-Dervout, Parallel computation of frontal polymerization, in *Proc. Parallel CFD95, Passadena*, edited by A. Ecer (North-Holland, Amsterdam, 1995), 23.
7. M. Garbey and D. Tromeur-Dervout, Massively parallel computation of stiff propagating fronts, *Combust. Theory Modelling* **1–3**, 271 (1997).

8. M. Garbey, A. Taik, and V. Volpert, Influence of natural convection on stability of reaction fronts in liquid, *Quart. Appl. Math.*, to appear.
9. M. Garbey, A. Taik, and V. Volpert, Linear stability analysis of reaction fronts in liquid, *Quart. Appl. Math.* **54**(2), 225 (1996).
10. D. Gottlieb and R. Hirsh, Parallel pseudospectral domain decomposition techniques, *J. Sci. Comput.* **4**(4), 309 (1989).
11. D. Gottlieb and S. Orszag, *Numerical Analysis of Spectral Methods: Theory and Applications*, C.B.M.S.-N.S.F. Conference Series in Applied Mathematics, Vol. 26 (SIAM, Philadelphia, 1977).
12. M. Israeli, L. Vozovoi, and A. Averbuch, Spectral multidomain technique with local fourier basis, *J. Sci. Comput.* **8**(2), 135 (1993).
13. M. Israeli, L. Vozovoi, and A. Averbuch, Domain decomposition methods with local fourier basis for parabolic problems, *Contemp. Math.* **157** (1994).
14. M. Israeli, L. Vozovoi, and A. Averbuch, Spectral multidomain technique with local fourier basis, *J. Sci. Comput.* **9**(3), 311 (1994).
15. S. B. Margolis, H. Kaper, G. Leaf, and B. Matkowsky, Bifurcation of pulsating and spinning reaction fronts in condensed two-phase combustion, *Combin. Sci. Technol.* **43**, 127 (1985).
16. I. P. Nagy, L. Sike, and J. Pojman, Thermochromic composite prepared via a propagating polymerization front, *J. Am. Chem. Soc.* **117** (1995).
17. J. Pojman and I. Epstein, Convective effects in chemical waves. 1. Mechanism and stability criteria, *J. Phys. Chem.* **94**(12), 4966 (1990).
18. J. Pojman, R. Graven, A. Khan, and W. West, Convective instabilities in traveling fronts of addition polymerization, *J. Phys. Chem.* **96**, 7466 (1992).
19. V. Volpert, V. Volpert, S. Davtyan, I. Magrabova, and N. Surkov, Two-dimensional combustion modes in condensed flow, *SIAM J. Appl. Math.* **52**, 368 (1992).
20. V. Volpert, A. Volpert, and A. Merzhanov, Analysis of nonunidimensional combustion regimes by bifurcation theory methods, *Dokl. Phys. Chem.* **263**, 239 (1982).
21. A. Volpert, V. Volpert, and V. Volpert, Traveling wave solutions of parabolic systems, AMS, *Transl. Math. Monographs*, Vol. 140, Am. Math. Soc., Providence, RI, 1994.